Theoretical and measured underwater noise from surface wave orbital motion

Douglas H. Cato
Defence Science and Technology Organisation, P. O. Box 706, Darlinghurst, NSW 2010, Australia

(Received 4 October 1988; accepted for publication 24 September 1990)

This paper develops a theory of sound generation by orbital motion of sea surface waves (as distinct from motion directly resulting from wave breaking such as bubble oscillation) and compares the noise predictions with measurements in a carefully controlled experiment. Theory and measurement were found to agree within the experimental errors. The mechanism is also known as the nonlinear interaction of surface waves and has been addressed by a number of authors. The approach of this paper differs from other models in that it avoids the use of the commonly applied perturbation expansion, and calculates the total noise field whereas others have limited their estimates to sound production from standing waves and waves that closely approximate standing waves. It is shown that while standing waves result in distributed dipoles with vertical axes, other wave interactions result in dipoles with axes inclined to the vertical so that there are components with both horizontal and vertical axes. The relative contribution of the horizontal dipole components to the noise field is of the same order of magnitude as that of the vertical dipole components. This paper therefore predicts higher noise levels and different directionalities, and also determines the contribution from the evanescent or near field that dominates for receiver depths less than several hundred meters (depending on frequency) resulting in substantially higher noise levels at shallow receivers. On the basis of this and previous work there seems little doubt that this mechanism is a significant source of noise in the ocean, usually dominant from about 0.2 to 5 Hz.

PACS numbers: 43.30.Lz, 43.30.Nb

INTRODUCTION

This paper applies the theory of sound generation by moving fluid interfaces developed in a companion paper[1] to determine the underwater noise from orbital motion of the sea surface, that is, by wave motion as opposed to motion resulting directly from wave breaking (bubble oscillation, impact of spray, etc.). This mechanism is present whether or not the waves are breaking, and contributes at a much lower frequency than does the noise directly associated with wave breaking. This paper also reports the results of a carefully controlled experiment in a water supply reservoir to test the theory, and it is shown that the theory is capable of predicting noise levels to an accuracy within the errors of measurement. Some aspects of this paper have been presented elsewhere in abreviated form.[2,3]

This is, in effect, the mechanism that has come to be known as the nonlinear interaction of surface waves, although in fact there is no requirement for either the waves or their interaction to be nonlinear: only that there exists a nonlinear source term (like $u_i u_j$ in the theory below). All orbital motion of the sea surface generates sound,[1] but significant ensonification of the far field results only from the interaction of pairs of surface waves having wave numbers that are close to being equal in magnitude and opposite in direction, so that standing waves, or waves that very closely approach standing waves are produced. To a casual observer, the sea surface appears to be composed of waves traveling in almost the same direction, so that the production of standing waves seems most unlikely. But this is true only for the longest wavelength swell: measurements of the directional spectra of wind generated waves[4–9] show a substantial spread of energy in directions oblique to the wind and hence in waves traveling in opposite directions.

Sound generation by surface standing waves and the estimation of the noise field from interactions that can be closely approximated as standing waves has received more attention theoretically than perhaps any other mechanism in the vicinity of the sea surface. Miche[10] first showed that second-order pressure fluctuations of a standing wave do not attenuate with depth in contrast to the exponential decay of the first-order pressure fluctuations. Longuet-Higgins[11] developed this idea into a comprehensive theory of the generation of microseisms, and also provided an interpretation of the physical processes involved.[12] Brekhovskikh[13] applied this mechanism to the prediction of noise in the ocean, to be further developed with somewhat different approaches by Hughes,[14] Harper and Simpkins,[15] Lloyd,[16] and Kibblewhite and Wu.[17] The common theme in these works was the development of a perturbation expansion in which the first-order solution to the wave equation was the incompressible surface wave motion, and the second the acoustic field. Hughes questioned whether higher-order terms need to be included. The resulting noise predictions have characteristics that are broadly consistent with the few measurements available of noise in the deep ocean at the very low frequencies where this mechanism appears to be the dominant source of noise. Nichols,[18] Talpey and Worley,[19,20] Webb and Cox,[21] and Cotaras *et al.*[22] have provided such measure-

 0001-4966/91/031096-17$00.80

ments but there has been no direct comparison between theory and measurement, the main deficiency being the absence of wave height spectral measurements simultaneous with the noise measurements. Kibblewhite and Ewans,[23] however, measured wave height spectra simultaneously with microseismic spectra and found the distinctive relationship in spectral shape predicted by the theories. They also calculated the noise in the ocean from the microseismic spectra and showed it to be broadly consistent with theoretical expectations (see also Ref. 24).

In the theoretical work cited above, and in this paper, sea surface orbital motion is described by linear theory. This has recently been questioned by Guo[25] who considered that the theories could not adequately describe sound generation by wave interaction under conditions of wave breaking, because the surface can then no longer be described by linear theory. The evidence suggests, however, that linear theory is adequate for this purpose. Linear theory of deep water waves appears to work remarkably well even in high winds. For example, particle velocities have been observed to be consistent with linear theory under conditions of high winds and considerable wave breaking.[26] The theoretical dispersion relationship also appears to be generally consistent with typical ocean measurements.[27] These are the parameters that are needed for the theories. Linear theory is an approximation under any conditions: it is a matter of whether it is an adequate approximation, and it does appear so in this case. The reason may be that, at any instant, whitecaps cover only a few percent of the sea surface,[28] and their dimensions are small compared to the surface wavelengths at the frequencies where this mechanism is significant. Guo also considered that terms higher than second order would be required under conditions of wave breaking. This limitation does not apply to the present theory, since it does not use a perturbation expansion. However, application of this theory to the conditions addressed by the models that are limited to second-order terms does not result in large discrepancies, suggesting that higher-order terms contribute a relatively small amount.

The theory of this paper differs from previous work in two respects. Firstly, the acoustic model developed in Ref. 1 follows a different approach, avoiding the use of the perturbation expansion common to previous models. Secondly, it determines the total pressure field rather than that due only to standing waves and interactions that closely approximate standing waves, which others have effectively treated as standing waves. It will be shown that while standing waves produce distributed dipole sources with vertical axes, waves that are close to, but not quite standing waves produce dipoles with axes inclined to the vertical so that there are components with horizontal axes. Previous models would therefore be expected to underestimate actual noise levels and to predict somewhat different directionalities. Nevertheless, the under estimate in level in the depths of the ocean would not be large (no more than about 10 dB) because only wave interactions that are very close to being standing waves ensonify the far field (see Sec. I below). This would seem to have been adequate justification for employing this approximation, in view of the considerable theoretical simplification. However, this approximation would be inadequate where directionality of the noise field is important. The inadequacies become more significant for shallow receivers because the large length scales involved would result in significant contribution by the near field at depths less than about 1000 m (depending on frequency).

I. REVIEW OF SOUND GENERATION MECHANISM

This section examines the essential features of sound generation by sea surface orbital motion to show the differences between the theory of this paper and the other theories cited above.

The companion paper[1] derives an expression for the sound radiated by a moving fluid interface like the sea surface. If the surface moves so that the mass or momentum flux of a region of the surface fluctuates, then sound is generated. The sources can be represented as distributed monopoles and dipoles in place of the sea surface. In other words, these sources account for both sound generation and the effect of the surface on the radiation of the sound. On the assumption that the source distributions were statistically homogeneous in the horizontal plane, the sound pressure spectrum was then expressed in terms of the frequency wave-number spectrum of the mass or momentum flux, as appropriate, so allowing the integrals over the sea surface to be evaluated independently of source conditions. For the distributed dipole sources, the sound pressure spectrum at frequency ω and depth z is given by Eq. (48) of Ref. 1:

$$P(\omega,z) = \int_{-\infty}^{\infty} \Phi_{ijlm}(\omega,\mathbf{k}) H_{ij}(\omega,\mathbf{k},z) H^{*}_{lm}(\omega,\mathbf{k},z) \frac{d\mathbf{k}}{(2\pi)^2}, \tag{1}$$

where $\Phi_{ijlm}(\omega,\mathbf{k})$ is the power spectrum of $\rho u_i u_j$. The notation of Cartesian tensors is used where the subscripts i, j, l, m take the values 1,2, or 3 appropriate to the coordinate axes, and repetition of a subscript implies summation over these values. The vertical axis is given by $i = 3$, positive downwards. The coupling factor $H_{ij}(\omega,\mathbf{k},z)$ is a measure of the extent to which a source Fourier component ensonifies the noise field. Their values are determined in Sec. III of Ref. 1. Since the integration is to be taken over the surface S, which is the horizontal plane of the mean sea surface, $j = m = 3$ and we write H_{ij} as H_i. In this analysis, the distributed dipoles are given in terms of their Cartesian components, each component having its dipole axis in the appropriate coordinate direction. As a patch of the sea surface moves, the axis of the resulting dipole will be in the direction of the momentum that is being transported and thus there will, in general, be both horizontal and vertical dipole components (see Sec. I of Ref. 1). Note that this does not imply that there are horizontal or vertical dipoles at the sea surface, but rather that the sound generated and radiated by sea surface motion can be treated as equivalent to having horizontal and vertical dipole components, *in place of* the sea surface. The effect of the pressure release surface is included in this source representation.

Most of the theory of Sec. II of this paper is concerned with relating $\Phi_{ijlm}(\omega,k)$ to $\Omega(\omega')$, the frequency spectrum of the surface wave height ζ_3 (the vertical displacement of the sea surface) which is easily measured. This involves determining the spectra of $\rho u_i u_j$ by convolving the individual u_i spectra. However, others have shown that only a small band of wave numbers contribute significantly to the convolution integral (at least for a receiver in the deep ocean), and have made an approximation that considerably simplifies this integral, but as a consequence, limits the source mechanism to standing waves.

The principle behind this is given in the following analysis, based on Sec. IV of Ref. 1, which shows that sound generated by elements of the sea surface tends to destructively interfere producing an evanescent field except where there are Fourier components of the source spectrum with phase speeds equal to or greater than the speed of sound. This is illustrated in Fig. 1, which shows the moduli of the dipole coupling factors in Eq. (1) and it is evident that the values fall sharply as k exceeds ω/c and phase speeds become subsonic. Sea surface motion has phase speeds of the order of a few meters per second—very much less than the speed of sound—but very high phase speeds can arise in the spectrum of the nonlinear term $u_i u_j$ under conditions approaching standing wave production. Consider a surface wave Fourier component of u_i of the form $\psi' \exp[i(\omega' t + \mathbf{k}' \cdot \mathbf{y})]$ and one of u_j of the form $\psi'' \exp[i(\omega'' t + \mathbf{k}'' \cdot \mathbf{y})]$, with phase speeds $\omega'/k' \sim \omega''/k'' \ll c$ (the absence of boldface type indicates the magnitude of the vector). The product $u_i u_j$ will contain a component $\psi'\psi'' \exp[i(\omega t + \mathbf{k} \cdot \mathbf{y})]$, where $\omega = \omega' + \omega''$ and $\mathbf{k} = \mathbf{k}' + \mathbf{k}''$. Its phase speed ω/k approaches infinity as $k \to 0$, i.e., as $\mathbf{k}' \to -\mathbf{k}''$, so that in the limit the two wave components produce a standing wave (since frequency and wave number are uniquely related in surface waves[29]). Since the monopole source term is linear [Ref. 1, Eq. (14)], the source phase speeds will be comparable to those of the surface waves and there will be significant ensonification only at extremely shallow depths. The monopole term in fact accounts for the first order pressure fluctuations below surface waves.

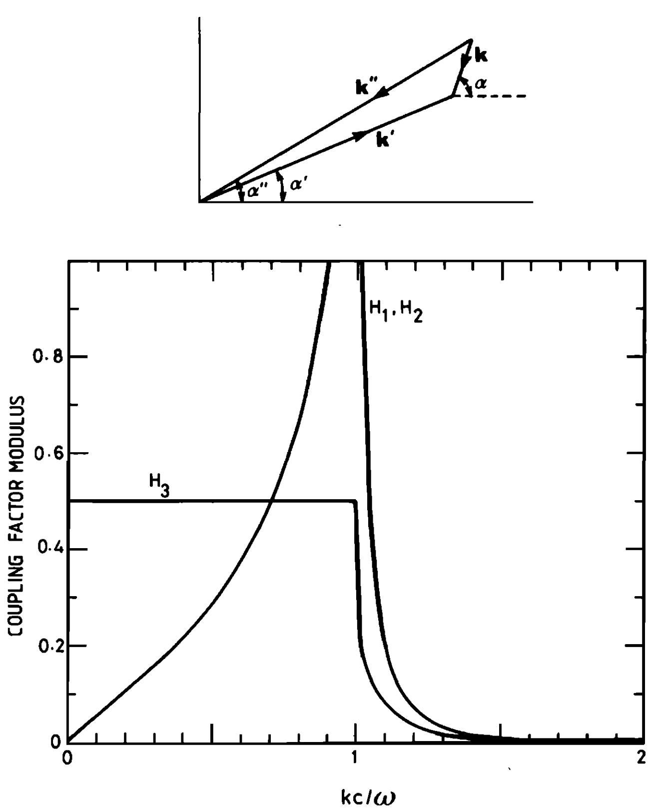

FIG. 1. Coupling factor moduli as functions of the nondimensional wave number of the source Fourier component. Here H_1, H_2 refer to the Cartesian component dipoles with horizontal axes (the maximum values, when axes are aligned parallel to $\mathbf{k}$, are shown); H_3 refers to the dipole components with vertical axes; and $\mathbf{k}'$ and $\mathbf{k}''$ are the wave numbers of the interacting surface waves.

Orbital motion of the sea surface induces correlated motion of the air and water on either side of the surface,[29] the velocities decaying exponentially with distance from the surface. It is shown in Ref. 1 (Sec. I) that the contribution to the noise field from the sound generated by this motion is negligible compared to that from motion of the surface itself (it would be at least 40 dB smaller). The reason is that these sources are quadrupole in nature and thus less efficient than the distributed dipoles of the surface motion, and the velocities decay very rapidly away from the surface. Turbulent motions of air or water are, of course, different sources.

In the frequency band containing most of the energy of surface waves, say from 0.1 to 100 Hz, waves numbers can differ in magnitude by no more than 2% if the phase speed of $u_i u_j$ is to be supersonic. As a consequence, previous models are based on the approximation $\mathbf{k}' = -\mathbf{k}''$, i.e., $k = 0$. The significance of this approximation is most readily examined in terms of the coupling factors $H_i(\omega, \mathbf{k}, z)$ which show specifically the extent to which the source spectral components ensonify the noise field. It is apparent in Fig. 1 that the values of H_1 and H_2, the coupling factors for the dipole components with horizontal axes, are zero when $k = 0$. Consequently, models based on the approximation $k = 0$ cannot account for the contribution from the horizontal dipole components which may be quite significant, especially in terms of the effect on the directionality of the noise field. (The singularity at $k = \omega/c$ applies to an infinite, nonabsorbing ocean and would result in infinite noise, but in a real ocean this would be replaced by a finite maximum.) The coupling factor H_3, for the dipole component with vertical axis, is independent of k for $k < \omega/c$. As it is the only coupling factor that is nonzero at $k = 0$, other models have found that the sources by this mechanism are vertical dipoles. The spatial average of the flux of horizontal momentum in a standing wave is zero, so it is to be expected that sound generation would be in the form of vertical dipoles only. In nonstanding waves, the flux of horizontal momentum does not average out spatially, so the dipoles will have horizontal components. Figure 1 can therefore be interpreted in terms of the relative contribution from the horizontal and vertical dipole components of sound generated when two surface waves interact.

Note that the values of the coupling factors in Fig. 1 drop sharply as k exceeds ω/c, i.e., as the phase speeds become subsonic. The values for $k > \omega/c$ decrease exponentially with receiver depth as $e^{-z(k-\omega/c)}$ whereas for $k < \omega/c$, they are independent of depth.[1] Thus in the depths of the ocean we can ignore the contribution for $k > \omega/c$. For shallow receivers this evanescent field is significant because length scales are the order of the acoustic wavelengths which are hundreds of meters at the frequencies where this mechanism is the dominant source. However, if the phase speeds are constrained to be of the order of those of the surface waves, as they are for the monopoles, k is so much larger than ω/c that the rate of decay with depth is too rapid for there to be a significant contribution at any practical receiver depth.

While other theories are not expressed in terms of coupling factors, the approach appears to be equivalent to calculating the contribution from the H_3 coupling factor (the vertical dipoles) only, and for $0 \leqslant k \leqslant \omega/c$. Although the integrals involved are evaluated over the range $k = 0$ to ω/c, the approximation $k = 0$ is made in the integrand, which is equivalent to considering wave interactions in this range as standing waves, with the consequence that only the contribution from the vertical component of the motion in the resultant wave is accounted for.

The well-established theory of linear surface waves in deep water ($k'd \gg 1$, where d is water depth) shows that frequency and wave number are uniquely related by the dispersion relationship[29]

$$\omega'^2 = gk' + Tk'^3/\rho, \tag{2}$$

where T is surface tension. The first term on the right-hand side dominates at frequencies below about 14 Hz, and the second at frequencies above 14 Hz. Below about 5 Hz the second term is negligible—the gravity wave regime—and we may write

$$\omega'^2 \approx gk'. \tag{3}$$

In deep water waves, particles move in circular orbits (in the vertical plane). Horizontal (in the direction of $\mathbf{k}'$) and vertical velocity components differ only in phase, and can be readily determined from the wave height. The velocity potential is of the form

$$\phi = \phi_0 \exp[-k'(y_3 - \zeta_3)] \exp[i(\omega' t - \mathbf{k}' \cdot \hat{\mathbf{y}})], \tag{4}$$

so that the velocity u_i is given in terms of the vertical surface displacement ζ_3

$$u_1 = i(k'_1/k')u_3 = i \cos \alpha' u_3, \tag{5}$$

$$u_2 = i(k'_2/k')u_3 = i \sin \alpha' u_3, \tag{6}$$

where

$$u_3 = \frac{\partial \zeta_3}{\partial t} \text{ (neglecting nonlinear terms)} \tag{7}$$

and α' is the angle $\mathbf{k}'$ makes with the y_1 axis.

In Appendix A we derive an expression for the spectrum of $u_i u_j$ in terms of the convolutions of the spectra of u_i and u_j. From this we obtain formally [see Eqs. (12) and (13) below] the relationships of the example above:

$$\omega = \omega' + \omega'', \tag{8}$$

$$\mathbf{k} = \mathbf{k}' + \mathbf{k}'', \tag{9}$$

where the prime or double prime symbols identify frequencies and wave numbers as those of the orbital velocities of the interacting waves, and the absence of primes identifies frequencies and wave numbers of the source term $\rho u_i u_j$. Since the values of the coupling factor moduli drop sharply as k exceeds ω/c, we may choose some value β such that significant ensonification of the noise field results only where $k \leqslant \beta\omega/c$.

For noise in the deep ocean $\beta = 1$, while for the near field $\beta = 5$ would be adequate for most practical receiver depths. The choice of $\beta = 5$ follows from examination of the behavior of the coupling factors in Ref. 1 as a function of nondimensional receiver depth $A = z\omega/c$. From Eq. (9) we expect that $|\mathbf{k}| \geqslant |\mathbf{k}'| - |\mathbf{k}''|$, so that this inequality is equivalent to

$$-\beta\omega/c \leqslant |\mathbf{k}'| - |\mathbf{k}''| \leqslant \beta\omega/c.$$

Using Eq. (3) this may be written

$$-\beta\omega/c \leqslant \omega'^2/g - (\omega - \omega')^2/g \leqslant \beta\omega/c,$$

which leads to

$$\omega/2 - \beta g/(2c) \leqslant \omega' \leqslant \omega/2 + \beta g/(2c).$$

Thus ω' differs from $\omega/2$ by no more than $\beta g/(2c)$, which is sufficiently small to write

$$\omega' \simeq \omega'' \simeq \omega/2. \tag{10}$$

Substituting $\omega' = \sqrt{gk'}$ in the inequality above gives

$$\omega^2/4 + \beta^2 g^2/(2c)^2 - \omega\beta g/(2c) \leqslant gk' \leqslant \omega^2/4 + \beta^2 g^2/(2c)^2 + \omega\beta g/(2c).$$

So for any chosen value of ω, k' can vary over a range of no more than $\omega\beta/c$ which, as a proportion of k', is

$$\omega\beta/(ck') = \omega\beta g/(c\omega'^2) \simeq 4\beta g/(\omega c) \simeq 0.004\beta/f,$$

where $\omega = 2\pi f$. Even at a frequency as low as 0.1 Hz, therefore, the possible variation in k' is only a few percent if $\beta \leqslant 5$. A similar result can be obtained for k''. Since $k = |\mathbf{k}' - \mathbf{k}''| \leqslant \beta\omega/c$,

$$k/k' \leqslant \beta\omega/(ck') \leqslant 4\beta g/(c\omega).$$

So k is a very small proportion of k' or k'' and

$$\mathbf{k}' \simeq -\mathbf{k}''. \tag{11}$$

We cannot, in general, use the approximations of Eqs. (10) and (11) without reducing the results in the analysis that follows to that for $k = 0$, the standing wave case. There will, however, be certain conditions where these approximations can be used without causing this limitation.

II. THEORETICAL DETERMINATION OF THE NOISE FIELD GENERATED BY SURFACE WAVE ORBITAL MOTION

A. Summary of procedure

Most of this section is concerned with relating $\Phi_{ijlm}(\omega,\mathbf{k})$, the power spectrum of $\rho u_i u_j$, to $\Omega_{33}(\omega')$, the power spectrum of the surface wave height ζ_3, which is readily measured. Here, $\Phi_{ijlm}(\omega,\mathbf{k})$ is first expressed as the convolution of $\Psi_{il}(\omega',\mathbf{k}')$ and $\Psi_{jm}(\omega'',\mathbf{k}'')$, the spectra of u_i and u_j, respectively, on the assumption that u_i and u_j are jointly Gaussian. The spectrum of u_i in polar coordinates $\Psi_{il}(\omega',k',\alpha')$ is then related to its wave-number spectrum $\chi_{il}(k',\alpha')$ by using the dispersion relationship [Eq. (3)]. By assuming that wave number and angular dependencies in the spectra of u_i, u_j are separable, each spectrum is expressed in terms of the wave-number (magnitude) spectrum $\chi_{il}(k')$ and its angular dependence $G(\alpha')$, which is given by empirical relationships.[5,6] It is also shown that constraints imposed by the dispersion relationship and the convolution integral result in there being only one value of k' for each value of α', so that the convolution integral reduces to an integral in α' only. Finally, Eqs. (5) to (7) are used to relate $\chi_{il}(k')$ to $\chi_{33}(k')$, which in turn is related to $\widehat{\Omega}_{33}(\omega')$, the spectrum of u_3 [using Eq. (3)], and then to $\Omega(\omega')$, the frequency spectrum of the surface wave height.

B. Determination of the spectrum of $\rho u_i u_j$ in terms of the spectra of u_i, u_j

Appendix A derives the following relationship between $\Phi_{ijlm}(\omega,\mathbf{k})$, the power spectrum of $\rho u_i u_j$, and $\Psi_{ij}(\omega,\mathbf{k})$, the spectrum of u_i, on the assumption that u_i and u_j are jointly Gaussian:

$$\Phi_{ijlm}(\omega,\mathbf{k}) = \rho^2\Psi_{il}(\omega,\mathbf{k})*\Psi_{jm}(\omega,\mathbf{k}) + \rho^2\Psi_{im}(\omega,\mathbf{k})*\Psi_{jl}(\omega,\mathbf{k}) \quad (12)$$

$$= \rho^2 \int\int_{-\infty}^{\infty} \Psi_{il}(\omega',\mathbf{k}')\Psi_{jm}(\omega-\omega',\mathbf{k}-\mathbf{k}')\frac{d\omega'\,d\mathbf{k}'}{(2\pi)^3} + \rho^2 \int\int_{-\infty}^{\infty} \Psi_{im}(\omega',\mathbf{k}')\Psi_{jl}(\omega-\omega',\mathbf{k}-\mathbf{k}') \times \frac{d\omega'\,d\mathbf{k}'}{(2\pi)^3}. \quad (13)$$

The first term on the right-hand side of Eq. (13) in polar coordinates is

$$[\Phi_{ijlm}(\omega,k,\alpha)]_1 = \rho^2 \int_{k'=0}^{\infty}\int_{\alpha'=0}^{2\pi}\int_{\omega'=-\infty}^{\infty} \Psi_{il}(\omega',k',\alpha') \times \Psi_{jm}(\omega-\omega',k'',\alpha'')\frac{k'\,dk'\,d\alpha'\,d\omega'}{(2\pi)^3}, \quad (14)$$

where $\mathbf{k}'' = \mathbf{k} - \mathbf{k}'$ and the absence of boldface type indicates the magnitude of the vector; and α', α'' are the angles which $\mathbf{k}'$, $\mathbf{k}''$, respectively, make with the y_1 axis, hence

$$k\cos\alpha = k'\cos\alpha' + k''\cos\alpha'', \quad (15)$$

$$k\sin\alpha = k'\sin\alpha' + k''\sin\alpha''. \quad (16)$$

Note that in Eq. (14) k'', α'' depend on k', α', respectively, although not explicitly shown.

Since ω' and k' apply to the orbital velocity u_i due to surface wave motion, they are uniquely related by Eq. (3). The same applies to $\omega'' = \omega - \omega'$ and k'' (but not, of course, to ω and k). Thus we define

$$\widehat{\omega}' = \widehat{\omega}'(k'), \quad (17)$$

$$\widehat{\omega}'' = \widehat{\omega}''(k'') \quad (18)$$

as the special values of ω' and ω'' determined by Eq. (3) given k', k'', respectively.

We now proceed to simplify the convolution integral of Eq. (14) by using Eqs. (15) to (18). Eventually we find that ω', ω'', k', and k'' can all be given as functions of α' alone, and by expressing this in forms of delta functions, two of the three integrals can be directly evaluated. We define the wave-number sepctrum of u_i as

$$\hat{\chi}_{il}(k',\alpha') = \int_{-\infty}^{\infty} \Psi_{il}(\omega',k',\alpha')\frac{d\omega'}{2\pi}. \quad (19)$$

Using Eqs. (17) and (18) this can be written

$$\Psi_{il}(\omega',k',\alpha') = \frac{1}{2}\hat{\chi}_{il}(k',\alpha')\left[\delta\left(\frac{\omega'-\widehat{\omega}'}{2\pi}\right) + \delta\left(\frac{\omega'+\widehat{\omega}'}{2\pi}\right)\right], \quad (20)$$

where $\delta(\ )$ is the Dirac delta function. Division by 2π in the delta function is necessary if Eq. (19) is to be satisfied by substitution of Eq. (20) and results from our definitions of power spectra which are density functions having unit bandwidth of one unit of $\omega/2\pi$ or one unit of $(k/2\pi)^2$ as the case may be. Note that the delta function in Eq. (20) imposes both the conditions expressed by Eqs. (17) and (18) since $\omega = \widehat{\omega}' + \widehat{\omega}''$.

In order to evaluate the convolution integral in the form shown in Eq. (14) we need to express k'' explicitly in terms of k, k', i.e., $k'' = |\mathbf{k} - \mathbf{k}'|$. This expression, and the dispersion relationship [Eq. (3)] result in k', k'' each having only one value for each value of α'.

To show this we note that

$$\omega = \widehat{\omega}'(k') + \widehat{\omega}''(k'') = \sqrt{gk'} + \sqrt{gk''} \quad (21)$$

and that ω and k are not variables in the convolution integral. Hence k' and k'' are not independent. If we express k'' in terms of k' using Eq. (21) and substitute for k'' in Eqs. (15) and (16), it would result in k' being dependent on α' and α'' only. Then we could express α'' in terms of k' and α' in Eq. (15) and substitute for α'' in Eq. (16). This would leave k' dependent on α' only. By similar procedure we could obtain k'' in terms of α' only. This can also be seen by reference to the vector diagram of Fig. 1. When k and α' are fixed, any increase in k' results in an increase in k'' and hence in ω by virtue of Eq. (21). Similarly a decrease in k' would result in a decrease in ω. But ω must remain fixed in the convolution integral, thus there is only one value of k', and only one value of k'' for each value of α'.

Hence

$$k'_\alpha = k'_\alpha(\alpha'), \quad (22)$$

$$k''_\alpha = k''_\alpha(\alpha'), \quad (23)$$

and using Eqs. (17) and (18)

$$\widehat{\omega}'_\alpha = \widehat{\omega}'_\alpha[k'_\alpha(\alpha')], \quad (24)$$

$$\widehat{\omega}''_\alpha = \widehat{\omega}''_\alpha[k''_\alpha(\alpha'')]. \quad (25)$$

These limitations lead to the following substitution in Eq. (14):

$$\Psi_{il}(\omega',k',\alpha')\Psi_{jm}(\omega'',k'',\alpha'') = \tfrac{1}{4}\hat{\chi}_{il}(k',\alpha')\hat{\chi}_{jm}(k'',\alpha'') \times \left[\delta\left(\frac{\omega'-\widehat{\omega}'}{2\pi}\right) + \delta\left(\frac{\omega'+\widehat{\omega}'}{2\pi}\right)\right]\delta\left(\frac{\widehat{\omega}'-\widehat{\omega}'_\alpha}{2\pi}\right). \quad (26)$$

The last delta function expresses the fact that k', which is always positive, is uniquely related to α'.

We now define $\chi_{il}(k')$, the one-dimensional wave-number spectrum (per unit $k/2\pi$) in terms of $\hat{\chi}_{il}(k',\alpha')$ the two-dimensional spectrum [per unit $(k/2\pi)^2$], on the assumption that the directional dependence is separable from the wave-number dependence,

$$\overline{u_i u_l} = \int_0^\infty \chi_{il}(k') \frac{dk'}{2\pi} \tag{27}$$

$$= \int_0^\infty \chi_{il}(k') \frac{dk'}{2\pi} \int_0^{2\pi} G(\alpha')d\alpha', \tag{28}$$

where

$$\int_0^{2\pi} G(\alpha')d\alpha' = 1. \tag{29}$$

Since Eq. (19) implies

$$\overline{u_i u_l} = \int_0^\infty \int_0^{2\pi} \hat{\chi}_{il}(k',\alpha') \frac{k'}{2\pi} d\alpha' \frac{dk'}{2\pi} \tag{30}$$

then

$$\hat{\chi}_{il}(k',\alpha') = 2\pi\chi_{il}(k')G(\alpha')/k'. \tag{31}$$

Substituting Eqs. (26) and (31) into Eq. (14) gives

$$\begin{aligned}
&[\Phi_{ijlm}(\omega,k,\alpha)]_1 \\
&= \frac{\rho^2}{2} \int_{k'=0}^\infty \int_{\alpha'=0}^{2\pi} \int_{\omega'=-\infty}^\infty \chi_{il}(k') \\
&\quad \times \chi_{jm}(k'')G(\alpha')G(\alpha'') \\
&\quad \times \left[\delta\left(\frac{\omega'-\hat{\omega}'}{2\pi}\right) + \delta\left(\frac{\omega'+\hat{\omega}'}{2\pi}\right)\right] \cdot \delta\left(\frac{\hat{\omega}'-\hat{\omega}'_\alpha}{2\pi}\right) \\
&\quad \times \frac{d\omega'\, dk'\, d\alpha'}{2\pi k''}
\end{aligned} \tag{32}$$

$$\begin{aligned}
&= \rho^2 \int_{\hat{\omega}'=0}^\infty \int_{\alpha'=0}^{2\pi} \chi_{il}[k'(\hat{\omega}')] \\
&\quad \times \chi_{jm}[k''(\hat{\omega}'')]G(\alpha')G(\alpha'') \\
&\quad \times \delta\left(\frac{\hat{\omega}'-\hat{\omega}'_\alpha}{2\pi}\right) \frac{1}{k''(\hat{\omega}'')} \frac{\partial k'}{\partial \hat{\omega}'} d\hat{\omega}'\, d\alpha',
\end{aligned} \tag{33}$$

where $(\partial k'/\partial\hat{\omega}')\, d\hat{\omega}'$ has been substituted for dk'. This leads to

$$\begin{aligned}
&[\Phi_{ijlm}(\omega,k,\alpha)]_1 \\
&= 2\pi\rho^2 \int_{\alpha'=0}^{2\pi} \chi_{il}(k'_\alpha)\chi_{jm}(k''_\alpha)\, G(\alpha')G(\alpha'') \\
&\quad \times \frac{1}{k''_\alpha(\alpha'')} \frac{\partial k'_\alpha}{\partial \hat{\omega}'_\alpha} d\alpha'.
\end{aligned} \tag{34}$$

This is the first term of Eq. (13). By analogy we can obtain a similar expression for the second term with the subscripts im and jl replacing il and jm, respectively.

C. Expression for the sound pressure spectrum

Using Eq. (34), the right-hand side of Eq. (13) can be evaluated and substituted into Eq. (1) to give the received sound pressure spectrum [after dropping the subscript α in Eq. (34)]. The result is

$$\begin{aligned}
P_D(\omega) &= \int_{-\infty}^\infty 2\pi\rho^2 \int_{\alpha'=0}^{2\pi} [\chi_{il}(k')\chi_{jm}(k'') \\
&\quad + \chi_{im}(k')\chi_{jl}(k'')] \\
&\quad \times \frac{G(\alpha')G(\alpha'')}{k''} \frac{\partial k'}{\partial \hat{\omega}'} d\alpha'\, H_{ij}(\omega,\mathbf{k},z) \\
&\quad \times H^*_{lm}(\omega,\mathbf{k},z) \frac{d\mathbf{k}}{(2\pi)^2}.
\end{aligned} \tag{35}$$

From the discussions leading to Eqs. (10) and (11) it is apparent that, for any chosen value of ω, the variables k'_α, k''_α, and ω' can vary by only a very small proportion of their values for significant ensonification of the noise field, and so may be considered to be constant in the integrals of Eq. (35). Also, since $G(\alpha'')$ varies relatively slowly with α', and $k' \simeq k''$ [Eq. (11)], it is acceptable to make the substitution $G(\alpha')G(\alpha'') \simeq G(\alpha')G(\alpha'+\pi)$, even though in general we cannot make the approximation $\mathbf{k}' \simeq -\mathbf{k}''$ [for the reasons given after Eq. (11)]. After changing to polar coordinates, k and α, and substituting $j=m=3$, as appropriate to our model, Eq. (35) becomes

$$\begin{aligned}
P_D(\omega) &= \rho^2 \frac{1}{k''} \frac{\partial k'}{\partial \hat{\omega}'} \int_0^{2\pi} \chi_{il}(k')\chi_{33}(k'')G(\alpha')G(\alpha'+\pi)d\alpha' \int_0^{k_0} \int_0^{2\pi} H_i(\omega,k,\alpha,z)H^*_l(\omega,k,\alpha,z)k\, d\alpha \frac{dk}{2\pi} \delta_{il} \\
&\quad + \rho^2 \frac{1}{k''} \frac{\partial k'}{\partial \hat{\omega}'} \int_0^{2\pi} \chi_{i3}(k')\chi_{3l}(k'')G(\alpha')G(\alpha'+\pi)d\alpha' \int_0^{k_0} \int_0^{2\pi} H_i(\omega,k,\alpha,z)H^*_l(\omega,k,\alpha,z)k \frac{d\alpha\, dk}{2\pi} \delta_{il}.
\end{aligned} \tag{36}$$

The Kronecker delta δ_{il} appears because the integration of $H_i H^*_l$ with respect to α over the range 0 to 2π is zero unless $i=l$, since $H_1 \propto \cos\alpha$, $H_2 \propto \sin\alpha$, and H_3 is independent of α [Eqs. (73)–(75) of Ref. 1].

From Eqs. (5)–(7) and (27) we obtain

$$\begin{aligned}
\chi_{11}(k') &= \cos^2\alpha' \cdot \chi_{33}(k'), \\
\chi_{22}(k') &= \sin^2\alpha' \cdot \chi_{33}(k'), \\
\chi_{13}(k') &= \cos\alpha' \cdot \chi_{33}(k'), \\
\chi_{23}(k') &= \sin\alpha' \cdot \chi_{33}(k').
\end{aligned} \tag{37}$$

We define the (one-sided) frequency spectrum of u_3

$$\overline{u_3 u_3} = \int_0^\infty \hat{\Omega}_{33}(\omega') \frac{d\omega'}{2\pi}, \tag{38}$$

and with this and Eq. (27) we obtain

$$\hat{\Omega}_{33}(\omega') = \frac{\partial k'}{\partial \omega'} \chi_{33}(k').$$

Since $u_3 = \partial\zeta_3/\partial t$ [Eq. (7)], we obtain the frequency spectrum $\Omega(\omega')$ of the wave height ζ,

$$\Omega(\omega') = \frac{1}{\omega'^2} \frac{\partial k'}{\partial \omega'} \chi_{33}(k'). \tag{39}$$

Combining this with Eqs. (37) to (39) gives

$$\chi_{il}(k') = g_{il}(\alpha')\Omega_{33}(\omega')\frac{\partial\omega'}{\partial k'}\omega'^2, \tag{40}$$

where

$$\begin{aligned} &g_{11}(\alpha') = |\cos^2\alpha'|, \quad g_{22}(\alpha') = |\sin^2\alpha'|, \\ &g_{33}(\alpha') = 1, \quad g_{13}(\alpha') = |\cos\alpha'|, \\ &g_{23}(\alpha') = |\sin\alpha'|. \end{aligned} \tag{41}$$

Inspection of Eq. (41) shows that

$$g_{il}(\alpha')g_{33}(\alpha'+\pi)\delta_{il} = g_{i3}(\alpha')g_{l3}(\alpha'+\pi)\delta_{il}. \tag{42}$$

Thus both terms of Eq. (36) are identical and this equation may be written

$$\begin{aligned} P_D(\omega) = 2\rho^2 \frac{\widehat{\omega}'^4}{k''}\frac{\partial\widehat{\omega}'}{\partial k'}\Omega^2(\widehat{\omega}')I_{\alpha_{il}} \\ \times\int_0^{k_0}\int_0^{2\pi} H_i(\omega,k,\alpha,z)H_l^*(\omega,k,\alpha,z) \\ \times k\frac{d\alpha\, dk}{2\pi}\delta_{il}, \end{aligned} \tag{43}$$

where

$$I_{\alpha'_{il}} = \int_0^{2\pi} g_{il}(\alpha')g_{33}(\alpha'+\pi)G(\alpha')G(\alpha'+\pi)d\alpha'. \tag{44}$$

The directional distribution of surface wave energy $G(\alpha')$ [defined by Eqs. (27) and (28)] has been the subject of a number of investigations.[4–9] Generally, a reasonable fit to the data in most cases is provided by the following expression, originally suggested by Longuet-Higgins *et al.*:[4]

$$G(\alpha') = N|\cos^{2s}\{(\alpha'-\alpha'_0)/2\}|, \tag{45}$$

where N is a normalizing factor to ensure that

$$\int_0^{2\pi} G(\alpha')d\alpha' = 1.$$

Maximum energy is in the wind direction indicated by α'_0 and by choosing $\alpha'_0 = 0$, we align the y_1 axis with the wind direction. Then

$$N = \left[\int_0^{2\pi}\left|\cos^{2s}\left(\frac{\alpha'}{2}\right)\right|d\alpha'\right]^{-1} = \frac{2^{2s-1}\Gamma^2(s+1)}{\pi\Gamma(2s+1)} \tag{46}$$

after integrating by parts. The parameter s indicates the extent to which energy is spread over α'.

Equation (44) can now be evaluated using Eqs. (41), (45), and (46) with $\alpha'_0 = 0$.

$$\begin{aligned} I_{\alpha_{33}} &= N^2\int^{2\pi}\left|\cos^{2s}\left(\frac{\alpha'}{2}\right)\cos^{2s}\left(\frac{\alpha'}{2}+\frac{\pi}{2}\right)\right|d\alpha \\ &= \frac{N^2}{2^{2s-1}}\int_0^{\pi}\sin^{2s}(\alpha')d\alpha' \\ &= \frac{N^2}{2^{2s-1}}\frac{\pi\Gamma(2s+1)}{2^{2s}\Gamma^2(s+1)} \text{ after integrating by parts} \\ &= \frac{\Gamma^2(s+1)}{2\pi\Gamma(2s+1)}. \end{aligned} \tag{47}$$

Similarly, using Eq. (47)

$$\begin{aligned} I_{\alpha_{22}} &= \frac{N^2}{2^{2s-1}}\int_0^{\pi}\sin^{2s+2}\alpha'\, d\alpha' \\ &= \frac{(2s+1)(2s+2)}{4(s+1)^2}I_{\alpha_{33}}, \end{aligned} \tag{48}$$

$$\begin{aligned} I_{\alpha_{11}} &= \frac{N^2}{2^{2s-1}}\int_0^{\pi}(1-\sin^2\alpha')\sin^{2s}\alpha'\, d\alpha' \\ &= I_{\alpha_{33}} - I_{\alpha_{22}}. \end{aligned} \tag{49}$$

Equations (73)–(78) of Ref. 1 show that, in the expressions for $H_i(\omega,k,\alpha,z)$, we can separate out the α dependence. Thus

$$H_i(\omega,k,\alpha,z) = \widehat{H}_i(\omega,k,z)h_k(\alpha)\delta_{ik}, \tag{50}$$

where

$$h_1(\alpha) = \cos\alpha, \quad h_2(\alpha) = \sin\alpha, \quad h_3(\alpha) = 1, \tag{51}$$

Then the integral with respect to α in Eq. (43) is

$$\begin{aligned} &\int_0^{2\pi} H_i(\omega,k,\alpha,z)H_l^*(\omega,k,\alpha,z)d\alpha \\ &= \widehat{H}_i(\omega,k,z)\widehat{H}_l^*(\omega,k,z)\int_0^{2\pi} h_k(\alpha)h_n(\alpha)d\alpha\,\delta_{ik}\delta_{ln} \end{aligned} \tag{52}$$

$$= \widehat{H}_i(\omega,k,z)\widehat{H}_l^*(\omega,k,z)\pi(1+\delta_{i3}). \tag{53}$$

Substituting Eq. (53) into (43) gives

$$\begin{aligned} P_D(\omega) = \rho^2\frac{\widehat{\omega}'^4}{k'}\frac{\partial\widehat{\omega}'}{\partial k'}\Omega^2(\widehat{\omega}')I_{\alpha_{il}} \\ \times\int_0^{k_0}\widehat{H}_i(\omega,k,z)\widehat{H}_l^*(\omega,k,z)k \\ \times dk\,\delta_{il}(1+\delta_{i3}). \end{aligned} \tag{54}$$

For $\widehat{\omega}' \leqslant 10\pi$ (acoustic frequencies of 10 Hz or less) Eq. (3) is a good approximation to the dispersion relationship and $k'' = \widehat{\omega}''^2/g$, $\partial\widehat{\omega}'/\partial k' = g/(2\widehat{\omega}')$. Also from Eq. (10) it will be acceptable to substitute $\omega/2$ for $\widehat{\omega}'$ or $\widehat{\omega}''$ and $\Omega(\omega/2)$ for $\Omega(\widehat{\omega}')$. Noting also that $\widehat{H}_1 = \widehat{H}_2$, we then obtain the expression for the received sound pressure spectrum at depth z,

$$\begin{aligned} P_D(\omega) = \frac{\rho^2 g^2}{4}\omega\Omega^2\left(\frac{\omega}{2}\right)\Bigg((I_{\alpha_{11}}+I_{\alpha_{22}})\int_0^{k_0}\widehat{H}_1\widehat{H}_1^* k\,dk \\ + 2I_{\alpha_{33}}\int_0^{k_0}\widehat{H}_3\widehat{H}_3^* k\,dk\Bigg). \end{aligned} \tag{55}$$

Alternatively as $I_{\alpha_{33}} = I_{\alpha_{11}} + I_{\alpha_{22}}$,

$$\begin{aligned} P_D(\omega) = \frac{\rho^2 g^2}{4}\omega\Omega^2\left(\frac{\omega}{2}\right)I_{\alpha_{33}}\Bigg(\int_0^{k_0}(\widehat{H}_1\widehat{H}_1^* \\ + 2\widehat{H}_3\widehat{H}_3^*)k\,dk\Bigg), \end{aligned} \tag{56}$$

where

$$I_{\alpha_{33}} = \Gamma^2(s+1)/2\pi\Gamma(2s+1).$$

Note that in the form of Eq. (55), $I_{\alpha_{11}}$ and $I_{\alpha_{22}}$ give the relative contribution from the dipoles with horizontal axes in the direction of the wind and normal to the wind, respectively. For example, the component in the direction of the wind contributes 1 1/2 and 2 times that normal to the wind for $s = 1$ and $s = 2$, respectively.

Noting that $P_D(\omega)$ is the two-sided power spectrum, the corresponding (one-sided) sound pressure spectrum level (dB *re*:1 μPa^2/Hz) is

$$\mathrm{SL}(f) = 20\log\{\rho g \Omega(\omega/2)\} + 10\log\left(\omega I_{\alpha_{33}} \int_0^{k_0} (\hat{H}_1 \hat{H}_1^* + 2\hat{H}_3 \hat{H}_3^*) k\, dk\right) + 117 \quad (57)$$

$$= 205 + 2\mathrm{WL}(f/2) + 10\log\left(f I_{\alpha_{33}} \int_0^{k_0} (\hat{H}_1 \hat{H}_1^* + 2\hat{H}_3 \hat{H}_3^*) k\right) dk, \quad (58)$$

where $\mathrm{WL}(f/2) = 10\log(\omega/2)$ is the wave height spectrum level (dB *re*:1 m^2/Hz) and $f = \omega/(2\pi)$ is the acoustic frequency. Although $k_0 = \infty$, the exponential decrease in the values of $\hat{H}_1$ and $\hat{H}_3$ as k_0 exceeds ω/c allows some finite value to be substituted for k_0 to acceptable accuracy. In the far field corresponding to a receiver on the bottom in the deep ocean, $k_0 = \omega/c$ is adequate.

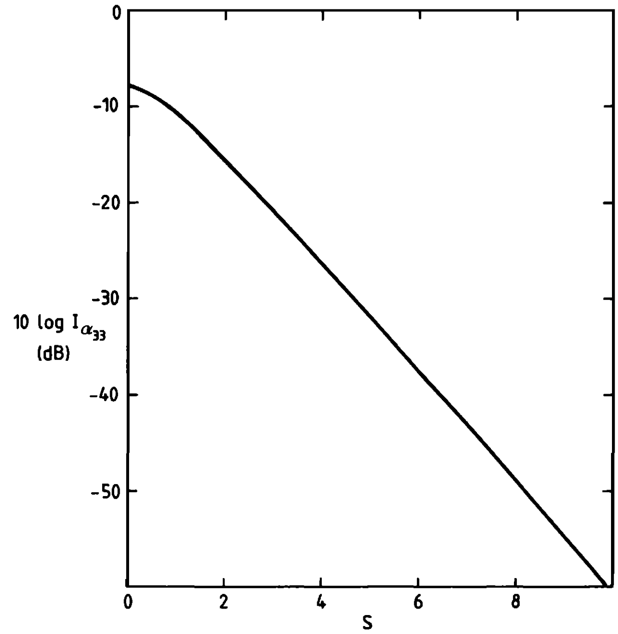

FIG. 2. The dependence of noise level on the surface wave-height spreading parameter s for values typical of those measured in the ocean [see Eq. (56)].

D. Interpretation of results

In common with all other models, Eq. (56) shows that the noise spectrum at any frequency is directly proportional to the wave height spectrum at half that frequency. Ocean waves have been extensively studied and for a steady, developed sea, the wave height spectrum has a very distinctive shape with a pronounced peak, below which the level falls very steeply. The simplest model of the spectrum above the spectral peak is the saturation spectrum of Phillips[29] in which the slope is ω^{-5}, and spectral levels are considered to have reached an upper limit as the result of a steady wind. More recent measurements have shown greater complexity. There is evidence of enhancement in level at the spectral peak[30] with a lesser slope of ω^{-4} for frequencies immediately above the region of enhancement, tending to ω^{-5} at higher frequencies.[9,31-33] We might expect the shape of the noise spectrum to be as distinctive as that of the wave height spectrum, but it will be somewhat modified by the variation with frequency of the directional spread of surface wave energy. This effect is shown in Fig. 2 as a plot of $10\log I_{\alpha_{33}}$ as a function of the spreading parameter s for values of s typical of those measured in the ocean. Most studies have shown that, for frequencies above the spectral peak, a reasonable fit to the data is provided by empirical models in which s is a function of nondimensional frequency $\tilde{f} = \omega' U/g$, where U is wind speed.[4-8] In two studies,[7,9] however, the authors prefer models in which the spreading depends on ω'/ω'_p, where ω'_p is the frequency at the spectral peak [Donelan[9] actually uses a model for the directional spreading which differs from Eq. (45)]. In all cases, however, as frequency decreases towards the spectral peak, the value of s increases and the value of $I_{\alpha_{33}}$ decreases. As an example, Fig. 3 shows the dependence of $10\log I_{\alpha_{33}}$ on nondimensional frequency $\tilde{f}$ using the model of Mitsuyasu *et al.*[6] in which $s = 11.5\tilde{f}^{-2.5}$. It is important to note that there is significant variation between models and this one is used only to show the general trend. However, it is apparent that the variation in s causes significant variation in $I_{\alpha_{33}}$ under typical ocean conditions. In addition, the variation between models, which increases as $\tilde{f}$ decreases, is sufficient to cause substantial variation in the noise prediction at frequencies near the spectral peak. For frequencies below the spectral peak, all studies indicate a dependence of s on ω'/ω'_p, with values decreasing with decreasing frequency. In general, the variation of $I_{\alpha_{33}}$ with $\tilde{f}$ can be expected to more than compensate for the peak enhancement in the wave height spectrum.

E. Comparison with the results of other theories

Because of the different theoretical approaches, a comparison of Eq. (56) with the results of other theories requires some manipulation to get the results in similar form. For this

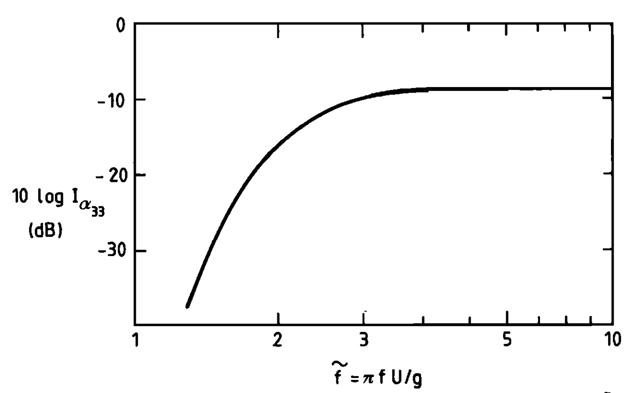

FIG. 3. The dependence of noise level on nondimensional frequency $\tilde{f}$ due to the variation in the spreading parameter s, using the model of Mitsuyasu *et al.*[6] for the dependence of s on $\tilde{f}$. Here, U is wind speed.

purpose, the results of Hughes[14] or Lloyd[16] are the most appropriate. The most direct comparison would be to consider only that part of the result of Eq. (56) that can be identified with the standing wave source addressed by the other theories, and to calculate the result as they did for the deep ocean where the near field component would not be significant. For standing waves, $\hat{H}_1 \hat{H}_1^* = 0$, and for the deep ocean, $\hat{H}_3 \hat{H}_3^* \simeq \frac{1}{4}$ for $k \leqslant \omega/c$ and may be considered to be negligible otherwise [Ref. 1, Eq. (99)]. Then Eq. (56) after integration from $k = 0$ to ω/c

$$P_D(\omega) = \frac{\rho^2 g^2}{16c^2}(\omega^3)\Omega^2\left(\frac{\omega}{2}\right)\int_0^{2\pi} G(\alpha')G(\alpha'+\pi)d\alpha'. \quad (59)$$

This can now be compared with Eq. (33) of Hughes[14] after making a correction of a factor of 2 (communicated by Hughes to Lloyd[16]) and noting that Eq. (59) is the two-sided power spectrum, and with the appropriate conversion between Hughes' wave-height, wave-number spectrum and $\Omega(\omega/2)$. The result is that Eq. (59) is a factor of π (5 dB) higher than Hughes' Eq. (33), as corrected, or Lloyd's result [Lloyd states his agreement with the corrected version of Hughes' Eq. (33)]. The reason for this difference is not clear. There may be some significance in the neglected higher-order terms of the perturbation expansion of these theories.

III. COMPARISON BETWEEN THEORY AND MEASUREMENT

A. The experiment

An experiment designed to rigorously test the theory was conducted at the hydrophone calibration facility in Woronora Dam, a water supply reservoir south of Sydney. This site was chosen because it provided much greater experimental control than is possible at sea, and interfering noise sources such as shipping were avoided. It also had the advantage that the frequencies of the wave-height spectrum were significantly higher that those usually observed in the open ocean. As a consequence, the values of the nondimensional frequency $\tilde{f}$ of Fig. 3 were in a range where there is little variation in the empirical models for the value of s (determined from measurements in open and enclosed waters), thus avoiding the uncertainty in estimating the value of $I_{\alpha_{33}}$ usual in predicting noise at sea.

Noise and wave-height spectra, and wind speed were measured simultaneously. Details of the instrumentation are given in Appendix B. Figure 4 shows a map of the dam with the position of the sensors, while Fig. 5 shows the instrumentation layout. A hydrophone and preamplifier were laid on the bottom in 35 m of water near the center of the water mass, about 100 m from a pontoon that contained the recording equipment, and from which the anemometer and wave staff were deployed. The bottom was mud overlaying sandstone. Considerable effort was made to minimize flow noise by use of fairings fitted to the cable and underwater components. About 250 m of cable was laid slack to cover the 100 m to the pontoon and the rise through the water column. The surface wave height was measured by detecting the changing capacitance between an insulated vertical wire and the surrounding water. This formed part of an electrical circuit so that changes in capacitance modulated the amplitude of a 5-kHz tone in proportion to the changes in the wave height. The wire was suspended 1.7 m from the pontoon on the windward side, using an aluminum pole of sufficient rigidity to ensure that mechanical resonances were well above the frequencies of interest. The position was well clear of the buoyancy tanks that supported the pontoon on either side, so that reflections from these were not important. The motion of the pontoon itself was shown to be of a frequency well below that of the lowest surface wave motion by training a video camera on the dam wall and observing the movement.

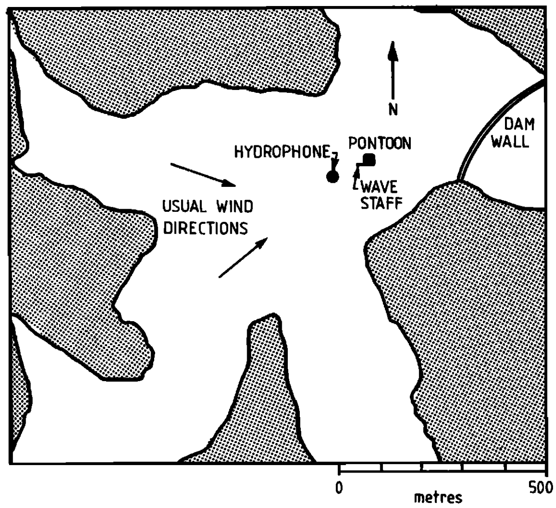

FIG. 4. Map of Woronora Dam showing the position of the sensors.

The systems were exhaustively calibrated both as components and as complete systems (Appendix B). The useable frequency range of the acoustic system was 0.1 Hz to about 30 kHz, the response being within $\pm$ 1 dB from 0.8 Hz to 2 kHz and 3 dB down at 0.33 Hz and 4 kHz. The wave-height system response was 3 dB down at 6 Hz. The signals were tape recorded on the pontoon and later synchronised and replayed to a Hewlett–Packard HP3582A dual channel analyzer that computed the fast Fourier transform for each set of data. Each spectrum was 128 point with an upper fre-

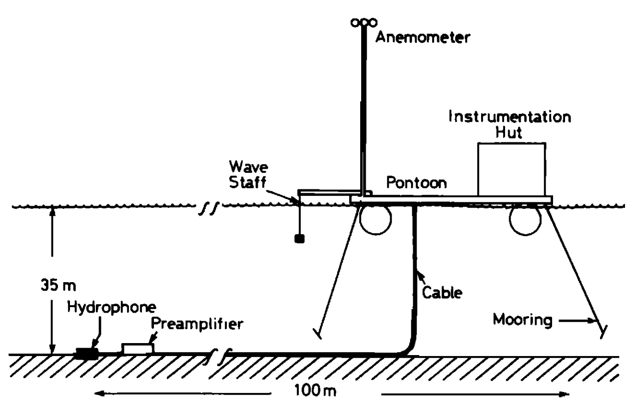

FIG. 5. Instrumentation layout for the measurements in Woronora Dam.

quency limit of 10 Hz and point spacing of 0.08 Hz. The results are presented as the average of a number of transforms each having a record length of 12.8 s. A Hanning window was used with an equivalent noise bandwidth of 0.12 Hz.

B. Noise prediction for Woronora Dam

The noise prediction was determined by evaluating Eq. (58) by substituting the simultaneous measurement of the wave-height spectrum. The coupling factors were evaluated numerically by taking the contributing area of sources to be circular with a radius of 400 m. Although the dam has quite an irregular shape, the choice of the area of sources is not critical, and as a variation of a factor of two in radius changes the prediction by an amount that is small compared with other uncertainties and experimental errors. The value of the spreading parameter s was taken as 1, appropriate to $\tilde{f} \geqslant 3$ observed. The variation in the observed values of s for $\tilde{f} \geqslant 3$ is small[4–8] and would account for a variation of no more than ± 1.5 dB in the noise prediction. The speed of sound used in the calculations was 1470 m/s, the average over the water column.

Numerical evaluation of the integral with respect to k in Eq. (58) showed that it was approximately proportional to ω^2. The expected slope of the noise spectra above the spectral peak would therefore be $2n - 3$, where n is the slope of the surface wave-height spectrum.

The effects of bottom reflections on the received noise level was estimated using the method of summation of surface- and bottom-reflected images given by Brekhovskikh.[34] In practice, of course, only a limited number of images needed to be included in the calculation because of the loss of energy on each bottom reflection. Successive terms in the calculation (incrementing by one surface and bottom reflection) tended to be out of phase because most of the phase change was due to the surface reflection. There was little phase difference due to the path difference because path lengths were generally smaller than a wavelength. The reflection loss and phase change were calculated by taking the density of the bottom to be 2.3×10^3 kg m^{-3}, and the compressional and shear wave speeds as 2744 and 1372 m/s, respectively. These values are appropriate to the sandstone strata with no overburden which underlies the dam. Although there is a layer of mud over the sandstone, its effect was assumed to be negligible because of the very small dimensions compared to a wavelength. The received pressure was calculated by summing coherently the incident and reflected pressure fields for the receiver on the bottom, allowing for the phase change along the propagation paths and at each reflection, and for the appropriate reflection losses. The appropriate dipole radiation beam patterns were also included in the calculations.

The results of these calculations is shown in Fig. 6 relative to the mean-square pressure from the direct path only, as a function of horizontal range. These calculations were made assuming that the bottom was horizontal. This, of course, is not the case. However, the bottom slope is small enough over much of the dam away from the perimeter for this to be a reasonable approximation, considering that the paths making the most significant contribution have reflections nearer the center. Irregularities in the bottom profiles would have negligible effect since their scales would be much less than a wave length. Figure 6 shows that the effect of the bottom is to cause an enhancement of up to 2 dB for sources close to the receiver and a reduction of up to 5 dB for distant sources. For sources close to the receiver, grazing angles at the bottom are high and the phase change is small, so that incident and reflected fields tend to augment. At long ranges, grazing angles are smaller and phase changes are sufficient to result in some destructive interference.

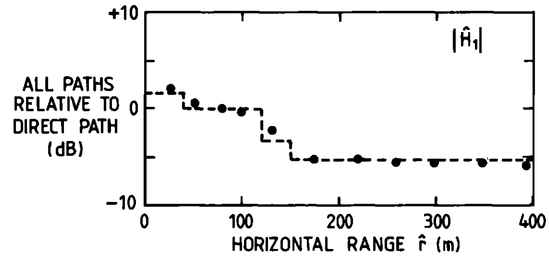

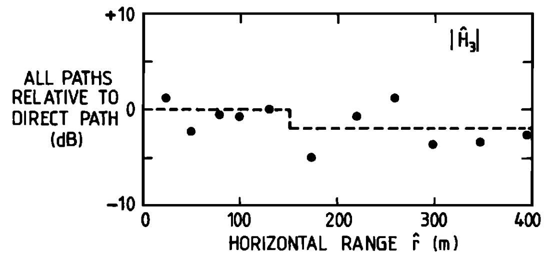

FIG. 6. Effect of bottom reflections on the level received from a source at the surface of Woronora Dam as a function of range. The source has dipole directivity appropriate to the coupling factor shown. The dots show the level by all paths relative to that by a direct path. The dashed line shows the value used to weight the coupling factor integrands.

In this theory, the effects of propagation appear in the coupling factor integrals (Sec. II of Ref. 1). The effect of bottom reflections was therefore estimated by weighting the integrands by a factor equal to the ratio of the contribution by all paths to that by the direct path only. This calculation was simplified by approximating this factor by its average value over range intervals where its variation was small, as shown by the dashed lines of Fig. 6. The results can be considered to provide approximate coupling factors that contain the contributions from both direct and reflected paths, as opposed to the original coupling factors that include the direct path only. Figure 7 shows the resulting coupling factor estimates, for direct path and all paths, obtained by numerical integration. The effect on the predicted noise level was obtained by substituting these results in Eq. (58) and numerically integrating with respect to k. Comparison of results shows that the effect of boundary reflections is to reduce the noise levels from dipoles with horizontal axes (H_1) by about 1 dB, and to reduce the noise levels from dipoles from vertical axes (H_3) by less than 0.1 dB. Combining

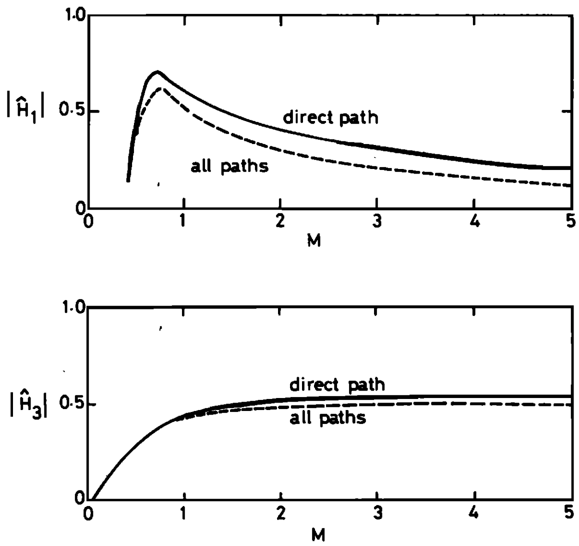

FIG. 7. Moduli of the coupling factors at 2 Hz as a function of $M = \omega/(kc)$ for Woronora Dam. "Direct path" shows the calculation for the direct path without boundary reflections. "All paths" is the result when boundary reflections are included.

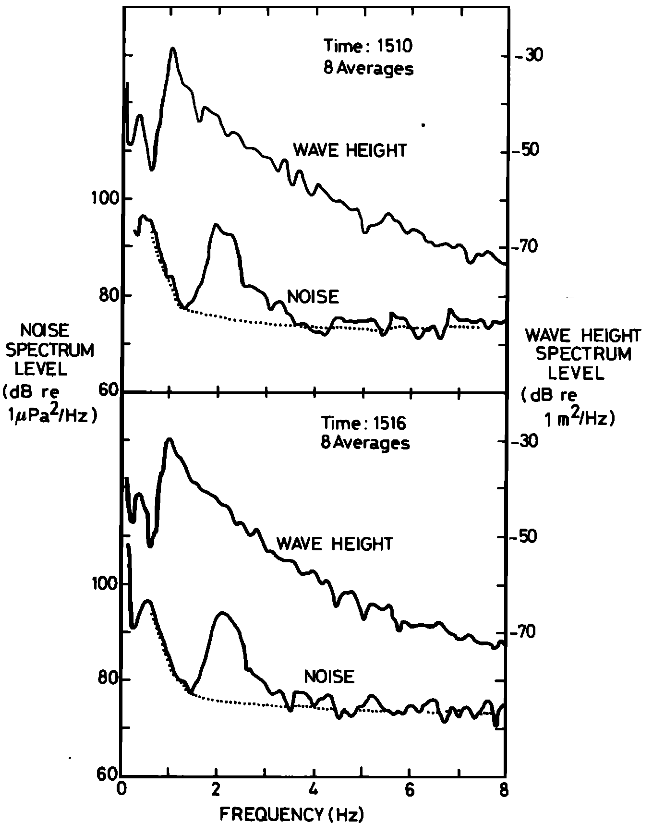

FIG. 8. Comparison of wave height and noise spectra measured simultaneously in Woronora Dam at the times shown on 12 August 1982. Total integration time: 102 s. The dotted line indicates the background noise measured on a day when the surface was smooth.

these results showed that the total noise level at 2 Hz is reduced by about 0.4 dB by the effects of boundary reflections. This effect is sufficiently small compared with errors of measurement to be ignored.

C. Results

To provide a suitable test of the theory, measurements were made at a time when the wind was comparatively steady over the extent of the dam and had been steady for sufficient time to produce a well developed surface wave field free of remnants of a previous field. Measurements were made under these conditions on 12 August 1982, after the wind had been steady for 5 h. Measurements were made on another occasion when there was no wind and the surface was smooth, to provide an estimate of the background in the absence of noise from surface motion.

Examples of simultaneous noise and surface wave-height spectra are shown in Figs. 8 and 9. The distinctive 2-to-1 ratio in the frequency of the peak in the noise spectra to that of the wave spectra is clearly evident. Ten such pairs of spectra measured at different times of day and for different integration times all clearly showed this effect. Close inspection of Figs. 8 and 9 shows that there is a small departure from the 2-to-1 ratio in frequencies, even allowing for the limitations imposed by the analysis frequency resolution of 0.08 Hz. This may have been caused by small temporal and spatial variations in the surface wave field as a consequence of small fluctuations in wind speed. The surface wave-height spectrum used in the calculation was measured at one position, whereas the noise spectrum results from an effect of surface wave height integrated over the whole water mass. Small departures of the local wave-height spectrum from the average over the water surface could be expected to give small discrepancies in the results. The departure from the 2-

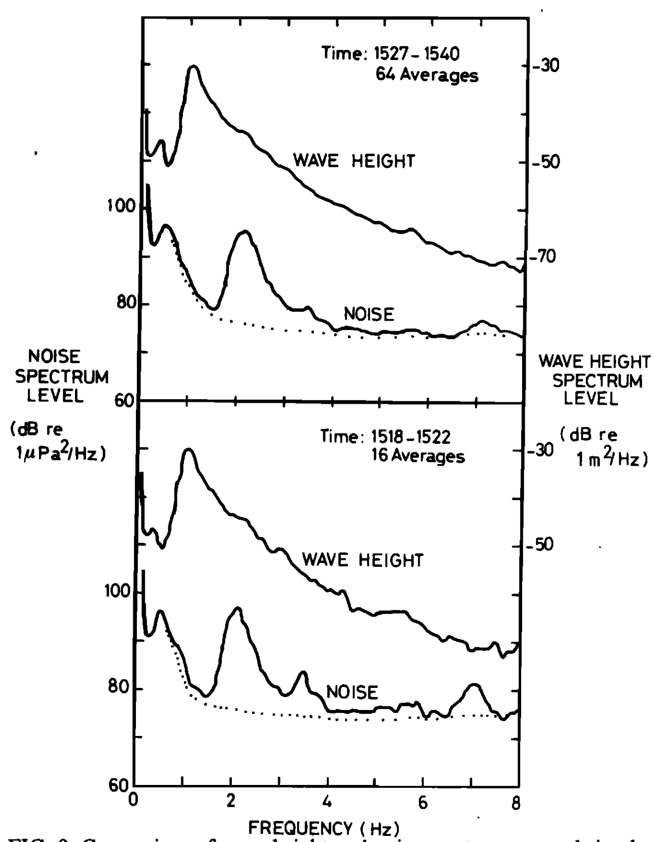

FIG. 9. Comparison of wave height and noise spectra measured simultaneously in Woronora Dam integrated over the times shown on 12 August 1982. The dotted line indicates background noise measured when the surface was smooth.

to-1 frequency ratio decreases as integration time increases, consistent with this explanation.

On other days when the wind was not steady there was sometimes evidence of two or three peaks in the wave-height spectrum, e.g., as the result of a change in the wind direction producing a new surface wave field, and there were corresponding peaks at approximately double these frequencies in the noise spectrum.

Figures 10 and 11 show comparisons between the measured noise spectrum and that predicted using Eq. (58) with the simultaneous measurement of the wave height spectrum. The results are in good agreement, not only in terms of the distinctive spectral shape but also in terms of the actual noise levels. For the longer integration times (Fig. 11) the measurements and theory differ by less than the experimental errors (allowing for the effects of background noise). The larger discrepancies for the shorter integration times (Fig. 10) are consistent with the larger uncertainty associated

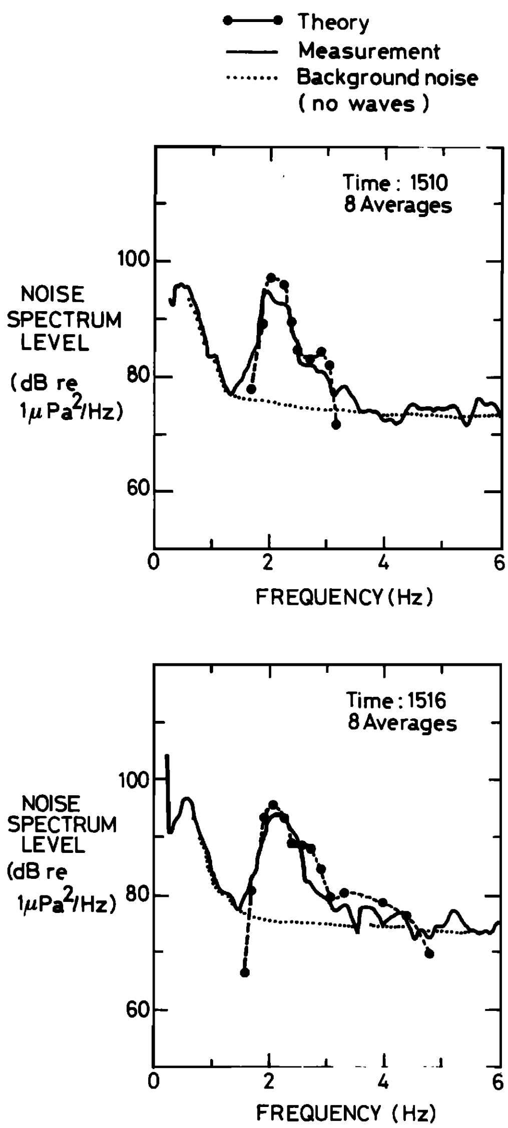

FIG. 10. Comparison between the measured noise spectrum and the theoretical prediction calculated from the simultaneous measurement of wave height spectrum, for the data of Fig. 8.

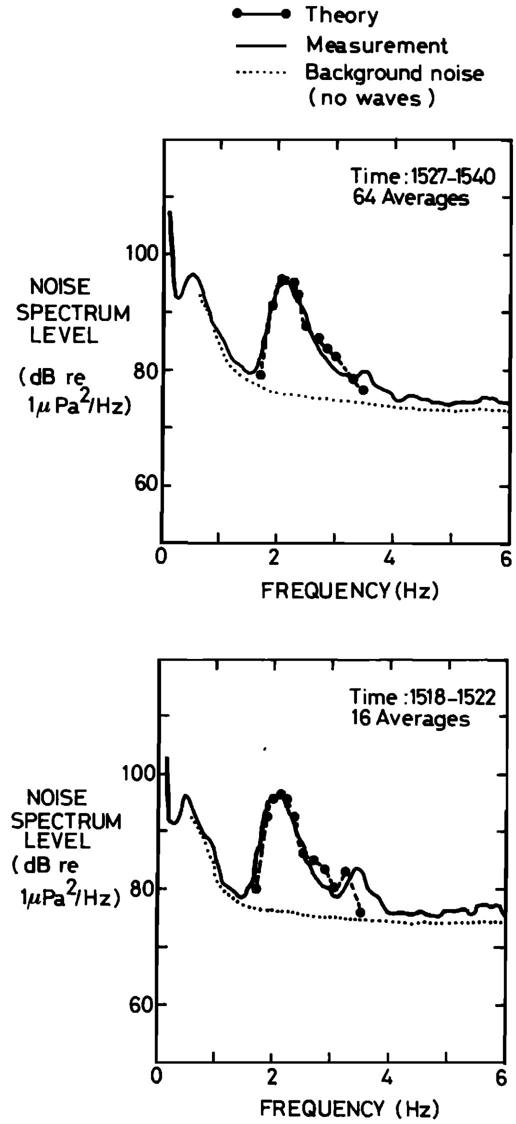

FIG. 11. Comparison between the measured noise spectrum and the theoretical prediction calculated from the simultaneous measurement of wave-height spectrum, for the data of Fig. 9.

with the Fourier transform estimate and small spatial and temporal fluctuations in the surface wave fields due to small fluctuations in wind speed, as discussed above. The better agreement for longer integration times would seem to justify the assumptions of stationarity (and ergodicity) and statistical homogeneity used in the theory. This good agreement between theory and measurement is due in part to the much greater experimental control compared with measurements at sea. It was easy to choose conditions of constant developed wave field over the entire water surface, the effects of propagation could be determined, the actual wave-height spectrum was known, and there was little uncertainty in the value of s at the frequencies and winds speeds of measurement. This is a particularly stringent test of the theory, since both the distinctive spectral shape and the noise levels had to be correctly predicted and there is little room for variation in the theoretical prediction as a result of uncertainties in the parameters included in the theory.

The receiver depth in Woronora Dam is sufficiently shallow for there to be significant contribution from the near field. The relative contributions of the near and far fields are in the proportion of approximately 80:20, so that ignoring the near would have resulted in an underestimate in the noise prediction of about 6.5 dB. The relative contributions of the horizontal and vertical dipole components are in the proportion of approximately 60:40. The total noise level exceeds what would be predicted by other theories by about 15 dB, due to a large extent to the contributions from the near field and the horizontal dipole components.

IV. PREDICTION OF NOISE IN THE OCEAN

Since the noise spectrum depends on the square of the wave-height spectrum as well as on the directional spread of wave energy, it is apparent that any noise prediction depends critically on the chosen description of the surface wave height. From the discussion of Sec. II D, it is apparent that the variation between empirical models of the wave-height spectrum and the directional spread is sufficient to cause significant variation in the noise predictions. Different propagation conditions will also affect noise levels. Consequently any general prediction of noise without knowledge of the actual surface wave or propagation conditions can be no better than an order of magnitude estimate.

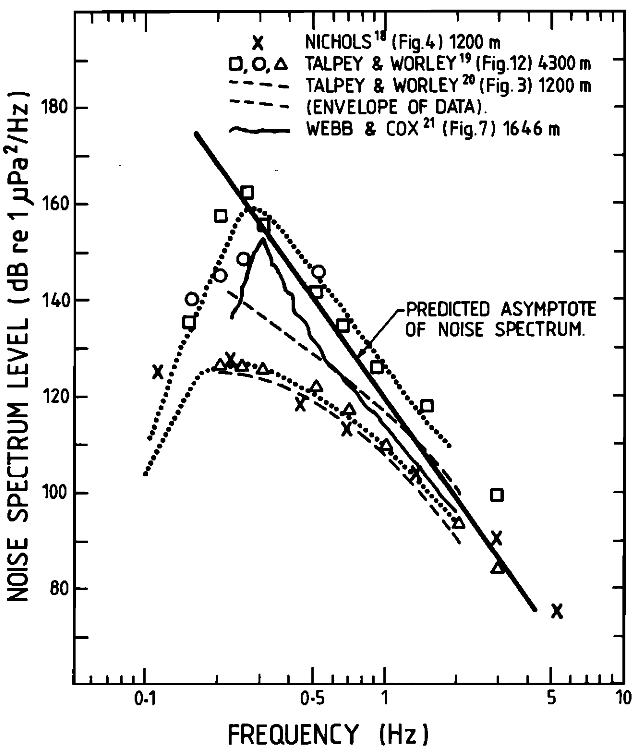

FIG. 12. Predicted asymptote of the far-field noise spectrum in a nonrefracting bottomless ocean. This was calculated from Eq. (58) using the saturated wave-height spectrum of Phillips[29] and the asymptotic value of $I_{\alpha_{33}}$ at high frequencies from Fig. 3. The spectrum would fall steeply at frequencies below the spectral peak at twice the frequency of the peak in the wave-height spectrum. Also shown are sets of ocean noise measurements at the depths shown (see key). The dotted lines show the envelope of the noise levels calculated by Kibblewhite and Ewans[23] from microseismic measurements.

The decreasing value of $I_{\alpha_{33}}$ as frequency decreases (Fig. 3) can be expected to reduce the slope of the noise spectrum as frequency approaches the spectral peak from above, by varying amounts according to the sea surface conditions. It would, therefore, seem useful to calculate an asymptote of the noise spectrum above the spectral peak, based on the asymptote of $I_{\alpha_{33}}$ at high frequencies. For this purpose, the saturated wave-height spectrum of Phillips[29] would be adequate as a description of the upper limit for a fully developed sea. Figure 12 shows such an asymptote of the noise spectrum for a receiver deep (say 5000 m) in a nonrefracting, bottomless ocean (propagation conditions can be expected to affect this result significantly in the real ocean). To the accuracy of the figure, the radius of the area of contributing sources, required in the calculation of the coupling factors in Eq. (58), can be considered to be between 100 and 1000 km. The actual noise spectrum would fall sharply below the spectral peak which would be at a frequency equal to twice that of the peak in the wave-height spectra. Also shown in Fig. 12 are some deep ocean noise measurements under varying conditions. The dotted lines mark the envelope of the noise spectra calculated from microseismic measurements near shallow water by Kibblewhite and Ewans.[23]

The prediction falls towards the upper range of measured values, a result which is to be expected. Levels observed would be higher in areas where propagation loss is low, for example, where the bottom reflectivity is high. Schmidt and Kuperman[35] show that bottom interaction can cause significant enhancement in noise levels at these frequencies. Lower levels would be expected where the surface waves are less than the "saturated" condition of a developed sea. For example, a falling sea after the wind has dropped would result in substantially lower noise levels. The decrease in the value of $I_{\alpha_{33}}$ below its high-frequency asymptote would also result in lower noise levels, and the difference may be quite substantial where values of s are high (e.g., at frequencies approaching the spectral peak). Indeed, the substantial variation in the measured values of s in the region of the spectral peak is sufficient to vary the noise prediction by as much as 30 dB at frequencies near the spectral peak in typical ocean conditions. This is enough to account for most of the variation in the observed noise levels, without allowing for the effects of varying propagation or wave height conditions. It is not clear to what extent this variation in the measured values of s is real or the result of experimental errors. As stated above, the relationship of Fig. 3 should be taken as no more than indicative of the trend, given the significant variability in the estimates of s. More accurate predictions of noise levels near the spectral peak must await a better understanding of the dependence of s on oceanic parameters.

The relative magnitude of the contributions from the dipole components with horizontal and vertical axes depends on the dimensions chosen for the radius of the region of contributing sources. The contribution to the mean-square pressure of the horizontal dipole components exceeds that from the vertical components by a factor which varies from approximately 3 to 4 as the radius varies from 100 to 1000 km, in this model of a nonrefracting, bottomless ocean.

This factor may change significantly if the effects of refraction and bottom conditions are included in the estimate. For a radius of 100 km (and a receiver depth of 5000 m), the predictions are about 10 dB higher than would be calculated from other models using the same wave height spectra and s value, and ignoring propagation effects.

The noise prediction of Fig. 12 applies to a receiver sufficiently deep for only the far-field contribution to be significant. The near field, however, contributes substantially at shallower receivers. The dependence of noise level on nondimensional depth $A = \omega z/c$ is shown in Fig. 13, and as a function of depth for various frequencies in Fig. 14 for a non refracting bottomless ocean. Figure 13 compares the relative contributions as functions of depth of (a) the dipole components with horizontal axes, (b) the dipole components with vertical axes, (c) the sum of all components, and (d) the near field only from all components. The actual source dipoles are the resultants of these components, so will have axes inclined to both vertical and horizontal, the actual axis direction being determined by the direction of the momentum that is being transported as a patch of the surface moves. As discussed in Sec. I, these sources are not to be considered as placed at or near the real sea surface: in this representation the sources are *in place of* the sea surface. More detailed discussion of the significance of these sources is given in Ref. 1. Although the near field may be considered an evanescent one and can be represented as a superposition of inhomogeneous waves, it results from the interference of acoustic waves from source elements of the surface and its depth dependence varies from $A^{-1/2}$ to A^{-2}, and its contribution persists to substantial depths. The predictions of Fig. 12, therefore, should be increased by the amounts shown in Fig. 14 for receivers at depths less than 5000 m. Again, the effects of bottom reflections and refraction may change the relative contributions significantly. The slow phase speed of the near field spectral components may couple significantly to the bottom.[35] Note that the differential change in level with frequency as depth decreases will tend to steepen the spectrum for shallow receivers, having the opposite effect of the variation in $I_{\alpha_{33}}$ with frequency.

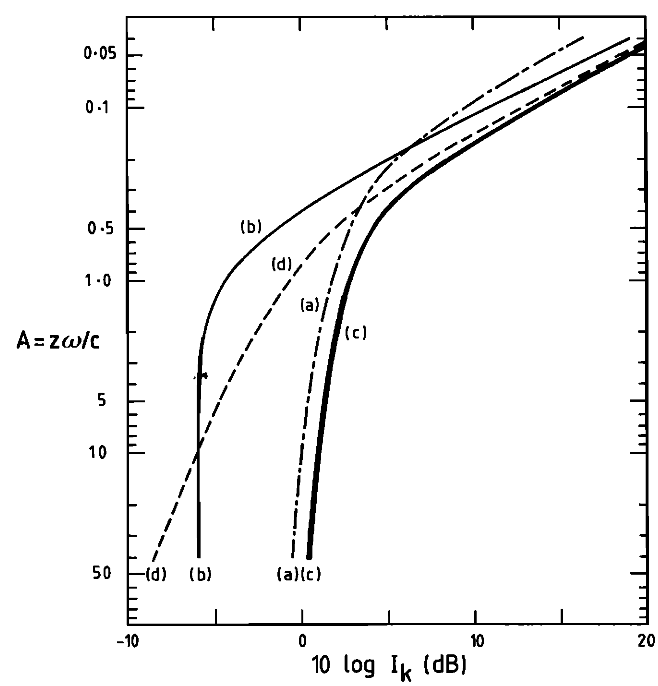

FIG. 13. Dependence of the noise field on nondimensional depth $A = \omega z/c$, for a nonrefracting, bottomless ocean. (a) $I_k = (c^2/\omega^2)\int_0^\infty \hat{H}_1 \hat{H}_1^* k\,dk$ (total field from horizontal dipole components); (b) $I_k = 2(c^2/\omega^2) \times \int_0^\infty \hat{H}_3 \hat{H}_3^* k\,dk$ (total field from vertical dipole components); (c) I_k = sum of integrals of (a) and (b) (total field, all components); (d) as for (c) but integrals evaluated from $k = 1$ to $k = \infty$ (total near field from all components).

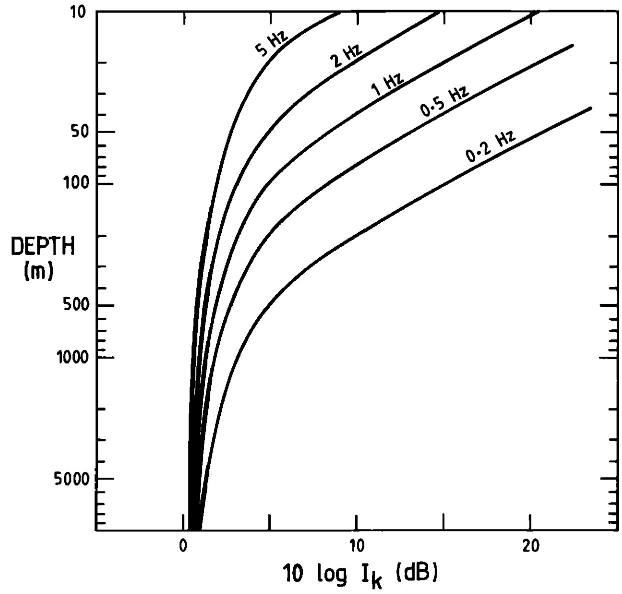

FIG. 14. Variation of noise level with depth for various frequencies, in a nonrefracting, bottomless ocean: $I_k = (c/\omega)^2\int_0^\infty (\hat{H}_1 \hat{H}_1^* + 2\hat{H}_3 \hat{H}_3^*) k\,dk$ [from Eq. (58)].

These predictions can be compared with those of other models of noise from this source mechanism for a non refracting bottomless ocean, and using the same wave-height spectra and values of the spreading parameter s. For a radius of 100 km, the predictions of this paper are about 10 dB higher for a receiver depth of 5000 m, and higher still by the additional amounts shown in Fig. 14 for shallower receivers. For a receiver at 100-m depth, for example, the excess would vary from about 12 to 25 dB over the frequency range of the prediction in Fig. 12.

V. CONCLUSIONS

This paper has applied a general theory of sound generation by fluid interfaces derived in Ref. 1, to determine the noise field from surface wave orbital motion, leading to the prediction of noise levels which agree with measured values to within the experimental errors. The agreement is unusually good for underwater acoustics noise predictions, but part of the success of this result is probably due to the fact that, in the enclosed waters of Woronora Dam where the measurements were made, significantly greater experimental control was possible than for measurements at sea. All parts of the system could be exhaustively tested and calibrated, and it was possible to choose conditions which closely mimicked the theoretical model.

The experiment was a particularly stringent test of the theory. Not just the noise levels, but also the very distinctive spectral shape, had to be adequately predicted. A rigorous test of the theory at sea awaits a controlled experiment in which both wave-height and noise spectra are measured simultaneously at a site where the propagation conditions are known. Ideally, the parameter s determining the spreading of the surface wave energy should also be measured (in the absence of a better model for predicting s). Theoretical predictions for the ocean, based on generalized wave-height spectra and ignoring the effects of refraction and bottom reflections, are broadly consistent with measurements at sea, and in particular the distinctive theoretical spectral shape is evident in the measurements. Two aspects of the theory which will be more difficult to test are the depth dependence in which much higher noise levels are expected in the near field and the directionality of the noise field dependent on the relative contribution of the dipole components with vertical axes and those with horizontal axes.

The predictions of this theory are broadly consistent with other theories of sound generation by wave–wave interaction, when due allowance is made for certain approximations in these other theories. Since this theory determines the noise from all orbital wave motion rather than approximating the source mechanism as standing waves, noise predictions are about 15 dB higher in Woronora Dam than would be predicted by other models and would also be expected to be of the order of 10 dB higher in the deep ocean depending on the particular propagation conditions (the larger difference in Woronora Dam is due to significant contribution from the near field). The most significant difference is in the noise directionality and the levels in the near field. Standing waves generate only dipoles with vertical axes whereas other wave interactions generate dipole components with both vertical and horizontal axes. The relative contribution of each depends on the propagation conditions, but generally they will be the same order of magnitude. An extended source like the sea surface is characterized by a near field or evanescent field which dominates for depths less than $A = z\omega/c = 1$, and has a depth dependence of $A^{-1/2}$ to A^{-2}. It accounts for the fact that there is significant destructive interference in the far field of sound waves generated by an extended source. Consequently, substantially higher noise levels are to be expected in the near field which may extend to several hundreds of meters at the frequencies where this mechanism is dominant. Noise levels at a depth of 100 m, for example, would be 12 to 25 dB higher (depending on frequency) than predicted by other models. The standing wave solution predicts only part of the far-field noise. When the theory of this paper is applied to standing waves, the results are close to those obtained by other models. This suggests that the contribution of the higher-order terms of the perturbation expansion, which were ignored in these other models, is small. In general it might be said that the approximations of earlier models were quite acceptable for their purpose, i.e., determining the order of magnitude of noise levels in the deep ocean. This paper offers more accurate estimates and also provides the basis for determining the noise directionality and the much higher noise levels to be expected for shallow receivers.

On the basis of this and previous work there seems little doubt that this mechanism is a significant source of ambient noise in the ocean, usually dominant in the frequency range from about 0.1 to 5 Hz, or, more specifically, from a frequency equal to twice the frequency of the peak in the surface wave height spectrum to the point where this steeply sloping spectrum falls below the next spectral component of ambient noise. There appear to be good prospects for accurately predicting the levels and directionality of noise generated by this mechanism. This will require the theory to be matched to suitable propagation models, and an adequate description of the surface wave conditions. The noise prediction depends critically on the wave-height spectrum and its spreading parameter s. As a consequence, there is considerable uncertainty in providing generalized estimates of noise because of the range in empirical models of surface wave-height spectra and in the wide variation in the measured values of s, especially near the spectral peak. More accurate predictions require a better understanding of the factors that determine the value of s.

ACKNOWLEDGMENTS

I am particularly indebted to Dr. Ian S. F. Jones for the many discussions and advice on aspects of the theory. I am also indebted to the following, who assisted in the design and deployment of the equipment. Jouko Uusioja, Frank Bruzzone, and Frank Harper gave valuable advice on the development of the electronic equipment and were responsible for some of the circuit designs. Brian Jones assisted by Tony Duffy developed the electronics for the noise recording system and assisted in the deployment. Frank Di Francesco assisted in the development of the wave staff and in the measurements, with careful attention to detail. George Gardiner, Shamus O'Brien, and Mark Savage developed the hardware. Lothar Schwertner operated the hydrophone calibration facility. Thanks are also due to Dr. Hiroshi Kawamura of Tohoku University for dynamically calibrating the wave staff, while visiting Sydney University.

APPENDIX A: RELATIONSHIP BETWEEN SPECTRUM OF $u_i u_j$ AND SPECTRUM OF u_i

Assuming that u_i and u_j are jointly Gaussian, fourth-order moments and products of second-order moments are related by[36]

$$\begin{aligned} E[x_1\ x_2\ x_3\ x_4] &= E[x_1\ x_2]E[x_3\ x_4] + E[x_1\ x_3]E[x_2\ x_4] \\ &\quad + E[x_1\ x_4]E[x_2\ x_3] - 2\bar{x}_1\cdot\bar{x}_2\cdot\bar{x}_3\cdot\bar{x}_4, \end{aligned} \tag{A1}$$

where $E[\quad]$ means the expected value of and $\bar{x}_1$ is the mean value of x_1. Having assumed that u_i and u_j are stationary and homogeneous, and choosing

$$\begin{aligned} &x_1 = u_i(t,\mathbf{y}), \quad x_2 = u_j(t,\mathbf{y}), \\ &x_3 = u_l(t+\tau,\mathbf{y}+\boldsymbol{\eta}), \\ &x_4 = u_m(t+\tau,\mathbf{y}+\boldsymbol{\eta}), \end{aligned} \tag{A2}$$

leads to

$$E[x_1 \ x_2] = \overline{u_i u_j}, \tag{A3}$$

$$E[x_1 \ x_3] = R_{il}(\tau,\boldsymbol{\eta}), \tag{A4}$$

and

$$E[x_1 \ x_2 \ x_3 \ x_4] = R_{ijlm}(\tau,\boldsymbol{\eta}), \tag{A5}$$

where $R_{il}(\tau,\boldsymbol{\eta})$ is the cross correlation function of $u_i(t,\mathbf{y})$ and R_{ijlm} is the cross correlation function of $u_i u_j$.

Substituting Eq. (A3)–(A5) into (A1) and taking the Fourier transform of both sides gives

$$\int\int_{-\infty}^{\infty} R_{ijlm} e^{i(\omega\tau - \mathbf{k}\cdot\boldsymbol{\eta})} d\tau\, d\boldsymbol{\eta}$$
$$= \int\int_{-\infty}^{\infty} \overline{u_i u_j} \cdot \overline{u_l u_m}\, e^{i(\omega\tau - \mathbf{k}\cdot\boldsymbol{\eta})}\, d\tau\, d\mathbf{n} + \int\int_{-\infty}^{\infty} R_{il}(\tau,\mathbf{n}) \cdot R_{jm}(\tau,\boldsymbol{\eta}) e^{i(\omega\tau - \mathbf{k}\cdot\mathbf{n})}\, d\tau\, d\mathbf{n}$$
$$+ \int\int_{-\infty}^{\infty} R_{im}(\tau,\boldsymbol{\eta}) \cdot R_{jl}(\tau,\boldsymbol{\eta}) e^{i(\omega\tau - \mathbf{k}\cdot\boldsymbol{\eta})}\, d\tau\, d\boldsymbol{\eta} - 2\int\int_{-\infty}^{\infty} \bar{u}_i \cdot \bar{u}_j \cdot \bar{u}_l \cdot \bar{u}_m e^{i(\omega\tau - \mathbf{k}\cdot\boldsymbol{\eta})}\, d\tau\, d\boldsymbol{\eta}. \tag{A6}$$

The means $\bar{u}_i$ and $\overline{u_i u_j}$ in the first and last terms of the right-hand side are constants in the integrals which are thus integral representations of the delta function. These terms are therefore zero unless $\omega = 0$ and $k = 0$, so may be ignored.

Then

$$\hat{\phi}_{ijlm}(\omega,\mathbf{k}) = \Psi_{il}(\omega,\mathbf{k})*\Psi_{jm}(\omega,\mathbf{k}) + \Psi_{im}(\omega,\mathbf{k})*\Psi_{jl}(\omega,\mathbf{k}) \tag{A7}$$

where $\hat{\Phi}_{ijlm}(\omega,\mathbf{k}) = \Phi_{ijlm}(\omega,\mathbf{k})/\rho^2$ is the power spectrum of $u_i u_j(t,\mathbf{y})$, $\Psi_{il}(\omega,\mathbf{k})$ is the power spectrum of $u_i(t,\mathbf{y})$, and * denotes convolution.

APPENDIX B: DETAILS OF INSTRUMENTATION

The hydrophone was a General Instrument Corporation Z3B and was connected to a stainless steel canister on the bottom by 4 m of cable. A further 250 m of cable connected the canister to the pontoon. The canister contained a preamplifier that was a modified version of a Princeton Applied Research model 185 normally used in their phase lock amplifier. It was used because of its very high input impedance and its exceptionally low electrical noise at very low frequencies. At 2 Hz this was equivalent to a sound pressure at the hydrophone of about 40 dB *re*: 1 μPa^2/Hz, and over the frequency range of interest was more than 35 dB below the lowest measured acoustic noise. The preamplifier was modified to include a power supply, calibration test signal and remote switching control. Acoustic data were recorded on the FM track of a Nagra IV-SJ tape recorder. The hydrophone was calibrated prior to deployment. After deployment, the performance of the acoustic system was checked *in situ* by projecting signals from the pontoon and comparing the result from a reference hydrophone, also suspended from the pontoon.

The wave-height recording system was based on a circuit reported by Anderson *et al.*,[37] with significant modifications. It measured the varying capacitance between an insulated vertical wire and the surrounding water. The capacitance varied in proportion to the amount of wire submerged and amplitude moduated a 5-kHz tone that was recorded on a Nagra III tape recorder. A 1-mm-diam enamel-coated wire was used, the effective capacitance being 2560 pF/m. The system was calibrated in the laboratory by causing the wire to oscillate vertically at a known rate through still water. System amplitude linearity was better than 1% over a wire length of 1.2 m.

[1] D. H. Cato, "Sound generation in the vicinity of the sea surface: source mechanisms and the coupling to the received sound field," J. Acoust. Soc. Am. **89**, 1076–1095 (1991).

[2] D. H. Cato, "Theoretical and measured noise from water wave orbital motion," Proc. 11th Int. Congr. Acoust., Paris, July 1983 **2**, 449–452 (1983).

[3] D. H. Cato and I. S. F. Jones, "Noise generated by motion of the sea surface - theory and measurement," in *Sea Surface Sound: Natural Mechanisms of Surface Generated Noise in the Ocean*, edited by B. R. Kerman (Kluwer, Dordrecht, 1988), pp. 391–402.

[4] M. S. Longuet-Higgins, D. E. Cartwright, and N. D. Smith, "Observations on the directional spectrum of sea waves using the motions of a floating buoy," in *Ocean Wave Spectra* (Prentice–Hall, Englewood Cliffs, NJ, 1963), pp. 111–136.

[5] G. L. Tyler, C. C. Teague, R. H. Stewart, A. M. Peterson, W. H. Munk, and J. W. Joy, "Wave directional spectrum from synthetic aperture observations of radio scatter," Deep Sea Res. **21**, 989–1016 (1974).

[6] H. Mitsuyasu, F. Tasai, T. Suhara, S. Mizuno, M. Ohkusu, T. Honda, and K. Rikiishi, "Observations of the directional spectrum of ocean waves using a cloverleaf buoy," J. Phys. Oceanogr. **5**, 750–760 (1975).

[7] D. E. Hasselmann, M. Dunckel, and J. A. Ewing, "Directional wave spectra observed during JONSWAP 1973," J. Phys. Oceanogr. **10**, 1264–1280 (1980).

[8] L. H. Holthuijsen, "Observations of the directional distribution of ocean-wave energy in fetch-limited conditions," J. Phys. Oceanogr. **13**, 191–207 (1983).

[9] M. A. Donelan, J. Hamilton, and W. H. Hui, "Directional spectra of wind generated waves," Philos. Trans. R. Soc. London Ser. A **315**, 509–562 (1985).

[10] M. Miche, "Mouvements ondulatoires de la mer en profondeur constante ou decroissante," Ann. Ponts Chauss. **114**, 25–78 (1944).

[11] M. S. Longuet-Higgins, "A theory of the origin of microseisms," Trans. R. Soc. London Ser. **243**, 1–35 (1950).

[12] M. S. Longuet-Higgins, "Can sea waves cause microseisms?" in *Proc. Symposium on Microseisms* (Harriman, New York, 1952).

[13] L. M. Brekhovskikh, "Underwater sound waves generated by surface waves in the ocean," Izv. Atmos. Ocean Phys. **2**, 582–587 (1966).

[14] B. Hughes, "Estimates of underwater sound (and infrasound) produced by nonlinearly interacting ocean waves," J. Acoust. Soc. Am. **60**, 1032–1039 (1976).

[15] E. Y. Harper and P. G. Simpkins, "On the generation of sound in the ocean by surface waves," J. Sound Vib. **37**, 185–193 (1974).

[16] S. P. Lloyd, "Underwater sound from surface waves according to the Lighthill–Ribner theory," J. Acoust. Soc. Am. **62**, 425–435 (1981).

[17] A. C. Kibblewhite and C. Y. Wu, "The generation of infrasonic ambient noise in the ocean by nonlinear interactions of ocean surface waves," J. Acoust. Soc. Am. **85**, 1935–1945 (1989).

[18] R. H. Nichols, "Infrasonic ambient ocean noise measurements: Eleuthera," J. Acoust. Soc. Am. **69**, 974–981 (1981).

[19] T. E. Talpey and R. D. Worley, in Ref. 18.
[20] T. E. Talpey and R. D. Worley, "Infrasonic ambient noise measurements in deep Atlantic water," J. Acoust. Soc. Am. **75**, 621–622 (1984).
[21] S. C. Webb and C. S. Cox, "Observations and modelling of sea floor microseisms," J. Gephys. Res. **91**, 7343–7358 (1986).
[22] F. D. Cotaras, I. A. Fraser, and H. M. Merklinger, "Near-surface ocean ambient noise measurements at very low frequencies," J. Acoust. Soc. Am. **83**, 1345–1359 (1988).
[23] A. C. Kibblewhite and K. C. Ewans, "Wave–wave interactions, microseisms and infrasonic ambient noise in the ocean," J. Acoust. Soc. Am. **78**, 981–994 (1985).
[24] A. C. Kibblewhite and C. Y. Wu, "A reexamination of the role of wave–wave interactions in ocean noise generation," J. Acoust. Soc. Am. **85**, 1946–1957 (1989).
[25] Y. P. Guo, "On sound generated by weakly nonlinear interactions of surface gravity waves," J. Fluid Mech. **181**, 311–328 (1987).
[26] G. Z. Forristall, E. G. Ward, V. J. Cardone, and L. E. Borgmann, "The directional spectra and kinematics of surface gravity waves in tropical storm Delia," J. Phys. Oceanogr. **8**, 888–909 (1978).
[27] O. M. Phillips, "The dispersion of short wavelets in the presence of a dominant long wave," J. Fluid Mech. **107**, 465–485 (1981).
[28] E. C. Monahan, "Oceanic whitecaps," J. Phys. Oceanogr. **1**, 139–144 (1971).
[29] O. M. Phillips, *The Dynamics of the Upper Ocean* (Cambridge U. P., Cambridge, 1977), 2nd ed.
[30] K. Hasselmann, T. P. Barnett, E. Bouws, H, Carlson, D. E. Cartwright, K. Enke, J. A. Ewing, H. Gienapp, D. E. Hasselmann, P. Kruseman, A. Meerburg, P. Muller, D. J. Olbers, K. Richter, W. Sell, and H. Walden, "Measurements of wind-wave growth and swell decay during the Joint North Sea Wave Project (JONSWAP)," Erganzung. Deutsch. Hydrograph. Z. Reihe A, 12 (1973).
[31] S. Kawai, K. Okada, and Y. Toba, "Field data support of three-seconds power law and $gu_* \sigma^{-4}$ spectral form for growing wind waves," J. Oceanogr. Soc. Jpn. **33**, 137–150 (1977).
[32] G. Z. Forristall, "Measurements of a saturated range in ocean wave spectra," J. Geophys. Res. **86**, 8075–8084 (1981).
[33] K. K. Kahma, "A study of the growth of the wave spectrum with fetch," J. Phys. Oceanogr. **11**, 1503–1515 (1981).
[34] L. M. Brekhovskikh, *Waves in Layered Media* (Academic, New York, 1960).
[35] H. Schmidt and W. A. Kuperman, "Estimation of surface noise source level from low-frequency seismoacoustic ambient noise measurements," J. Acoust. Soc. Am. **84**, 2153–2162 (1988).
[36] J. S. Bendat and A. G. Piersol, *Random Data: Analysis and Measurement Procedures* (Wiley–Interscience, New York, 1971), p. 92, Eq. (3.132).
[37] A. L. Anderson, D. J. Shirley, and L. H. Wilkins, "An improved capacitive wave staff for water surface wave measurements," Applied Research Labs., University of Texas, Report AS-71-1359 (1972).